

# Universal critical behavior of the 2d Ising spin glass

L. A. Fernandez,<sup>1,2</sup> E. Marinari,<sup>3,4</sup> V. Martin-Mayor,<sup>1,2</sup> G. Parisi,<sup>3,4</sup> and J. J. Ruiz-Lorenzo<sup>5,2</sup>

<sup>1</sup>*Depto. de Física Teórica I. Facultad de Ciencias Físicas. Universidad Complutense de Madrid. 28040 Madrid. Spain.*

<sup>2</sup>*Instituto de Biocomputación y Física de Sistemas Complejos (BIFI), 50018 Zaragoza, Spain.*

<sup>3</sup>*Dip. di Fisica and INFN-Sezione di Roma 1, Università La Sapienza, P.le A. Moro 2, I-00185 Rome, Italy.*

<sup>4</sup>*Nanotec-CNR, UOS Roma, Università La Sapienza, P.le A. Moro 2, I-00185, Rome, Italy.*

<sup>5</sup>*Depto. de Física and Instituto de Computación Científica Avanzada (ICCAEx), Univ. de Extremadura, 06071 Badajoz, Spain.*

(Dated: April 18, 2016)

We use finite size scaling to study Ising spin glasses in two spatial dimensions. The issue of universality is addressed by comparing discrete and continuous probability distributions for the quenched random couplings. The sophisticated temperature dependency of the scaling fields is identified as the major obstacle that has impeded a complete analysis. Once temperature is relinquished in favor of the correlation length as the basic variable, we obtain a reliable estimation of the anomalous dimension and of the thermal critical exponent. Universality among binary and Gaussian couplings is confirmed to a high numerical accuracy.

PACS numbers: 75.10.Nr, 71.55.Jv, 05.70.Fh

## I. INTRODUCTION.

Spin glasses [1] are a rich problem [2–7]. In particular the Ising spin glass in  $D = 2$  spatial dimensions poses questions of interest both for theory and for experiments. The system remains paramagnetic for any temperature  $T > 0$ , but the critical limit at  $T = 0$  has puzzled theorists for many years [8–36]. On the other hand recent experiments in spin glasses are carried out in samples with a film geometry [37–39]. The analysis of these experiments will demand a strong theoretical command.

In the limit  $T \rightarrow 0$  the physics of the system is dictated by the low energy configurations of the system. The nature of the coupling constants  $J$  becomes the ruling factor: if the  $J$  are discrete and non vanishing, an energy gap appears. Instead, the gap disappears if the couplings are allowed to approach with continuity the value  $J = 0$ . Several Renormalization Group (RG) fixed points appear at  $T = 0$ , depending on the nature of the couplings distribution [26]. However, most of these fixed points are unstable even for the tiniest positive temperature: the only remaining universality class is the one of the continuous coupling constants [28, 32–35] (the very same effect is found in the Random Field Ising model [40]).

The distinction between universality classes is unambiguous only in the thermodynamic limit. For finite systems of size  $L$ , samples with discrete couplings display a crossover at scale  $T_L^*$  between continuous ( $T \gg T_L^*$ ) and discrete behavior ( $T \ll T_L^*$ ). How  $T_L^*$  tends to zero for large  $L$  has been clarified only recently [33, 34] (see below).

Perhaps unsurprisingly given these complications, the critical exponents of the model are poorly known. For the thermal exponent  $\nu$  ( $\xi \propto T^{-\nu}$ , where  $\xi$  is the correlation length) we only have crude estimates,  $\nu \approx 3.5$  [28] (estimates can be given by using indirect methods, see below). Even worse, the anomalous dimension  $\eta$  has been till date impossible to estimate [28, 31, 34] (correlations decay with distance  $r$  as  $C(r) \sim 1/r^{D-2+\eta}$  for  $r \lesssim \xi$ ,

making  $\eta$  crucial for an out of equilibrium analysis [41–43]). Besides, little is known about corrections to the scaling exponent  $\omega$ .

Here, we remedy these state of affairs by means of large scale Monte Carlo simulations. Crucial ingredients are: (i) we consider both continuous and discrete coupling distributions; (ii) multi-spin coding methods (novel for Gaussian couplings) provide very high statistics; (iii) the non-linear scaling fields (whose importance was emphasized in Ref. [44]) cause severe problems in the finite size scaling close to  $T = 0$ , that we are able to solve [45]. We also obtain for the first time a precise numerical bound for the anomalous dimension,  $|\eta| < 0.02$ . This strongly supports the conjecture  $\eta = 0$ . Decisive evidence for universality follows from our computation of  $\omega$ . For Gaussian couplings we also obtain a precise estimate of  $\nu$ .

## II. MODEL AND OBSERVABLE QUANTITIES.

We consider the Edwards Anderson model on a square lattice of linear size  $L$ , with periodic boundary conditions, nearest neighbors interactions and Ising spins  $\sigma_{\mathbf{x}} = \pm 1$ . The coupling constants  $J_{\mathbf{x}\mathbf{y}}$  are quenched random variables. A *sample* is a given couplings realization. Thermal averages for a given sample are denoted as  $\langle \dots \rangle$ . The statistical average of thermal mean values over the couplings is denoted by an over-line. We consider two different kinds of coupling distributions,  $J_{\mathbf{x}\mathbf{y}} = \pm 1$  with 50% probability, and a Gaussian distribution with zero mean and unit variance. For later use, we note a *temperature symmetry*: in our problem  $T$  and  $-T$  are equivalent because of the symmetry  $J \leftrightarrow -J$  of the couplings distribution.

We consider real replicas: couples of spin configurations  $\{s_{\mathbf{x}}\}$  and  $\{\tau_{\mathbf{x}}\}$  evolving with the same couplings, but otherwise statistically independent. Let  $q_{\mathbf{x}} = s_{\mathbf{x}}\tau_{\mathbf{x}}$ .

The order parameter  $q$  and the Binder ratio  $U_4$  are

$$q = \sum_{\mathbf{x}} q_{\mathbf{x}} / L^2, \quad U_4 = \overline{q^4} / \overline{q^2}^2. \quad (1)$$

$G(\mathbf{r}) = \sum_{\mathbf{x}} \overline{q_{\mathbf{x}} q_{\mathbf{x}+\mathbf{r}}} / L^2$  is the overlap-overlap correlation function. From its Fourier transform  $\hat{G}(\mathbf{k})$  we compute the spin glass susceptibility  $\hat{G}(\mathbf{k}=0) = L^2 \overline{q^2}$  and the second moment correlation length  $\xi_L$  [46–49].

### III. FINITE SIZE SCALING.

Exactly at  $T = 0$  our two models behave very differently. In the Gaussian case, barring zero measure exceptions, the ground state (GS) is unique with a continuous spectrum of excitations. As a consequence, at  $T = 0$  and for any size  $L$ ,  $\overline{q^2} = 1$ . It follows that the anomalous dimension exponent  $\eta = 0$  and, according to our definition,  $\xi_L = \infty$ , even for finite  $L$ .

The  $J = \pm 1$  model is gapped, with a highly degenerate GS. At large distances the correlation function behaves as  $G(\mathbf{r}, T = 0) \sim q_{\text{EA}}^2 + A/r^{\theta_S}$ , implying  $\xi_L \sim L^{\theta_S/2}$ .  $\theta_S \approx 1/2$  [20, 29, 33] is the entropy exponent. This  $T = 0$  behavior extends up to the crossover scale  $T_L^* \sim L^{-\theta_S}$  [33]. In fact, Eqs. (3,4) below apply for this model only down to  $T \sim L^{-1/\nu} \gg L^{-\theta_S}$  [34].

The singular part of the disorder averaged free energy scales as

$$F_{\text{singular}}(\beta, h, L) \simeq L^{-D} f(u_h L^{y_h}, u_T L^{y_T}), \quad (2)$$

plus sub-leading terms. Here  $u_h$  and  $u_T$  are the scaling fields [44, 49, 50] associated respectively with the magnetic field  $h$  and with the temperature  $T$  (since our  $D = 2$  system is only critical at  $T = 0$ ) [51]. The scaling fields  $u_T$  and  $u_h$  are (asymptotically  $L$ -independent) analytic functions of  $h$  and  $T$  that will enter our analysis through the numerical determination of observables like  $\xi_L/L$ ,  $U_4$ ,  $q^2$ , ... Recalling the  $T \leftrightarrow -T$  symmetry, one can expand by obtaining  $u_T(T, h) = \hat{u}_T(T) + \mathcal{O}(h^4)$ , where  $\hat{u}_T(T) \simeq u_1 T(1 + u_3 T^2 + \mathcal{O}(T^4))$ , and  $u_h(T, h) = h^2 \hat{u}_h(T) + \mathcal{O}(h^4)$  with  $\hat{u}_h(T) = c_0 + c_2 T^2 + \mathcal{O}(T^4)$ .

In terms of the scaling fields the correlation length behaves as

$$\xi_L = L F_{\xi}(L^{1/\nu} \hat{u}_T) + \mathcal{O}(L^{-\omega}), \quad (3)$$

where at variance with  $\hat{u}_T$  and  $\hat{u}_h$ , the critical exponents  $\nu$  and  $\omega$  and the scaling function  $F_{\xi}$  are universal [52]. We follow Refs. [53–55] and we factor out the temperature dependency, finding:

$$\overline{q^2} = [\hat{u}_h(T)]^2 F_{q^2}(\xi_L/L), \quad U_4 = F_{U_4}(\xi_L/L). \quad (4)$$

In Eq. (4) we have neglected again corrections of order  $L^{-\omega}$ . The scaling functions  $F_{q^2}$  and  $F_{U_4}$  are universal.

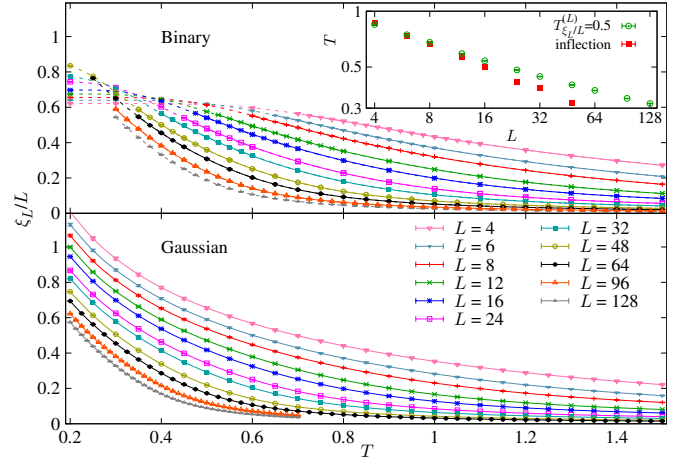


Figure 1. (color online) **Top:** Binary model correlation length (in units of the system size) versus temperature.  $\xi_L/L$  approaches its  $T = 0$  limit exponentially in  $1/T$  (because of the existence of an energy gap). We have an inflection point at  $T = T_{\text{inf}}^{(L)}$  (obtained from a cubic spline interpolation of  $\xi_L/L$ ), that we regard as a proxy for the crossover scale  $T_L^*$  [33]. At low  $T$  (discontinuous lines) we use less samples, see appendix A. **Inset:** Size evolution of the inflection points  $T_{\text{inf}}^{(L)}$  (red full squares), compared to  $T_{\xi_L/L=0.5}^{(L)}$  (open green circles). Data for binary model. As expected [34], the two temperature scales decouple for large  $L$ . **Bottom:**  $\xi_L/L$  vs.  $T$  for the Gaussian model does not show any crossover.

### IV. SIMULATION DETAILS.

High statistics was collected using 128-bits multi-spin coding (see [56] and appendix B). In the Gaussian case, the same bonds in the 128 copies of the system share the same absolute value of the couplings (only sign are at random and independent in different samples). Still, as shown in appendix B2, the statistical gain is significant. We have equilibrated [57] lattices of linear size  $L = 4, 6, 8, 12, 16, 24, 32, 48, 64, 96$  and 128 (see Figure 1 and appendix A).

### V. ON UNIVERSALITY.

Let us start with  $\xi_L$ . The Gaussian model, Fig. 1–bottom, displays the expected divergence upon approaching  $T = 0$ . In fact, the temperature where  $\xi_L/L = x$ , denoted  $T_{(\xi_L/L)=x}^{(L)}$  hereafter, decreases for larger sizes [Eq. (3) predicts  $T_{(\xi_L/L)=x}^{(L)} \sim L^{-1/\nu}$ , see below]. As for the binary model, see Fig. 1–top and inset, its  $\xi_L/L$  curves reflect the different behaviors above and below the temperature scale  $L^{-\theta_S}$  [33]. Here we do not investigate further the  $T \approx 0$  region nor this crossover.

Fortunately, universality emerges clearly if we bypass the temperature dependency as done in Eqs. (3,4).  $U_4$  at  $T_{\xi_L/L}^{(L)}$  reach an  $\xi_L/L$ -dependent universal limit for large

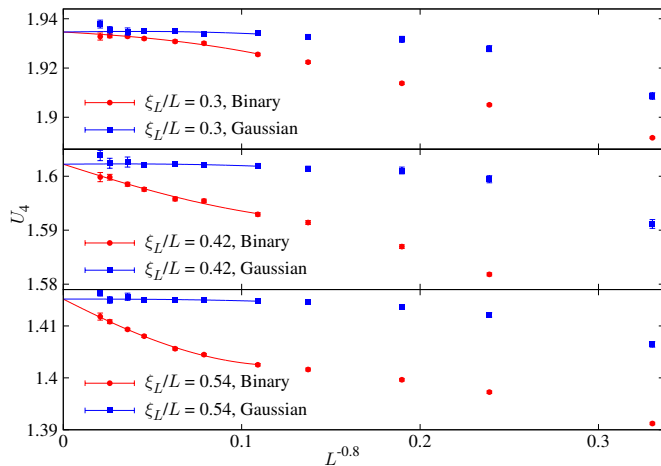


Figure 2. (color online) Binder ratio  $U_4$ , Eq. (1), at  $T$  where  $\xi/L = 0.3$  (**top**),  $0.42$  (**center**) and  $0.54$  (**bottom**) as a function of  $L^{-\omega}$  for the two models. The large  $L$  limit is model independent. The  $\omega$  exponent and the solid lines were obtained from a joint fit to Eq. (5).

values of  $L$ , as shown in Fig. 2. We compute the corrections to scaling exponent  $\omega$  from the behavior of  $U_4$ . One expects corrections to the leading behavior:

$$U_4^{(L)}(T_{\xi_L/L}^{(L)}) = F_{U_4}(\frac{\xi_L}{L}) + a(\frac{\xi_L}{L})L^{-\omega} + b(\frac{\xi_L}{L})L^{-(2-\eta)} \dots \quad (5)$$

The amplitudes  $a(\frac{\xi_L}{L}), b(\frac{\xi_L}{L})$  are model and  $\xi_L/L$ -dependent. If  $\eta=0$  analytic corrections are  $\mathcal{O}(L^{-2})$  [49].

We fit together binary and Gaussian data to Eq. (5) by standard  $\chi^2$  minimization, imposing a common  $F_{U_4}(\xi_L/L)$ . The goodness-of-fit estimator  $\chi^2$  is computed with the full covariance matrix, which limits the number of  $\xi_L/L$ -values that one may consider simultaneously in the fit.

In our fit to Eq. (5) we include data for  $\xi_L/L = 0.3, 0.42, 0.54$  and  $L \geq L_{\min}$ . We impose two requirements: (i) an acceptable  $\chi^2/\text{dof}$ ; (ii) stability in the fitted parameters upon increasing  $L_{\min}$ . We obtain  $\omega = 0.80(10)$  for  $L_{\min} = 16$ , with  $\chi^2/\text{dof} = 23.9/26$ . Interestingly, the amplitude  $a(\frac{\xi_L}{L})$  for the Gaussian model is compatible with zero for all values of  $\xi_L/L$ : the Gaussian model seems free of the leading corrections to scaling [58].

As a control of systematic errors, we evaluated a second fit imposing  $b(\frac{\xi_L}{L}) = 0$  and, for the Gaussian data, also  $a(\frac{\xi_L}{L}) = 0$ . We obtained  $\omega = 0.69(5)$  for  $L_{\min} = 32$  and  $\chi^2/\text{dof} = 14.3/23$ . Our final estimate is

$$\omega = 0.75(10)(5). \quad (6)$$

(first is the statistical error and second the systematic one).

## VI. THE ANOMALOUS DIMENSION.

Previous investigations have never succeeded in computing the anomalous dimension of the 2D spin glass. Our key idea is that Eq. (4) implies  $\eta = 0$ , provided that  $\hat{u}_h(T=0) \neq 0$  (traditional methods cannot handle the prefactor  $[\hat{u}_h(T)]^2$ , see appendix D).

We focus on the temperature dependence of  $\overline{\langle q^2 \rangle}$ , as computed at fixed  $\xi_L/L$ . For each  $L$  we choose  $T = T_{\xi_L/L}^{(L)}$ , see the two insets in Fig. 3. Eq. (4) tells that, apart from a constant  $F_{q^2}(\xi_L/L)$ , the curves should be smooth functions of  $T^2$ .

To compute the universal function  $F_{q^2}(\xi_L/L)$  we arbitrarily fix the scale  $(\xi_L/L) = 0.4$  (since, see Fig. 3, all our curves for  $\overline{\langle q^2 \rangle}$  at fixed  $\xi_L/L$  have some temperature overlap with the curve for  $(\xi_L/L) = 0.4$ ). We fit to a quadratic polynomial in  $T^2$  each curve  $\overline{\langle q^2 \rangle}$  at fixed  $\xi_L/L$  for an interval  $0 < T^2 < T_{\max, \xi_L/L}^2$ , see appendix A 2. We compute  $g(\xi_L/L) \equiv F_{q^2}(0.4)/F_{q^2}(\xi_L/L)$  as the ratio of the two  $T^2$ -fits, the one for a generic value of  $\xi_L/L$  and the fit for  $(\xi_L/L) = 0.4$ , as evaluated at  $T^2 = T_{\max, \xi_L/L}^2/2$ .

Our computation of the ratio  $g(\xi_L/L)$  respects three consistency tests: (i)  $g(\xi_L/L)$  turns out to be essentially model independent (Fig. 3); (ii)  $g(\xi_L/L) \sim (L/\xi_L)^2$  for small  $\xi_L/L$  (Fig. 3); (iii) the product of  $\overline{\langle q^2 \rangle}$  at fixed  $\xi_L/L$  with  $g(\xi_L/L)$  produces  $\xi_L/L$  independent curves. (Fig. 4).

Fig. 4 shows the (modified) scaling field  $[\hat{u}_h(T)]^2 F_{q^2}(0.4)$ . Given the  $T^2$  fits it is straightforward to extrapolate  $[\hat{u}_h(T)]^2 F_{q^2}(0.4)$  to  $T^2 = 0$  (dashed lines in Fig. 4). For both models the extrapolation is non-vanishing (implying  $\eta = 0$ ).

Finally, we obtain  $\eta = 0.00(2)$  from the scaling  $g(x) \sim x^{\eta-2}$  for small  $x = \xi_L/L$  ( $L \rightarrow \infty$  is taken at fixed  $x$ , see appendix C).

## VII. THE THERMAL EXPONENT.

The exponent  $\nu$  has never been successfully computed for this model [59]. RG suggests that  $1/\nu = -\theta$ , where  $\theta$  is the stiffness exponent controlling the size scaling of the change in the ground state energy when considering periodic and anti-periodic boundary conditions. Accurate determinations of  $\theta$  are available for the Gaussian model:  $-\theta = 0.281(2)$  [22],  $0.282(2)$  [24],  $0.282(3)$  [25] and  $0.282(4)$  [26]. A computation for the random anisotropy model yields  $\theta = 0.275(5)$  [30]. We shall obtain results of comparable accuracy for  $1/\nu$ . Due to the strong cross-over effects suffered by the binary model (see Fig. 1) we estimate  $1/\nu$  for the Gaussian model only.

We base our analysis on the determination of  $T_{\xi_L/L}^{(L)}$ . Even disregarding the leading universal corrections to scaling (see above our computation of  $\omega$ ), Eq. (3) predicts a rather complex behavior, with  $\hat{u}_T(T_{\xi_L/L}^{(L)}) =$

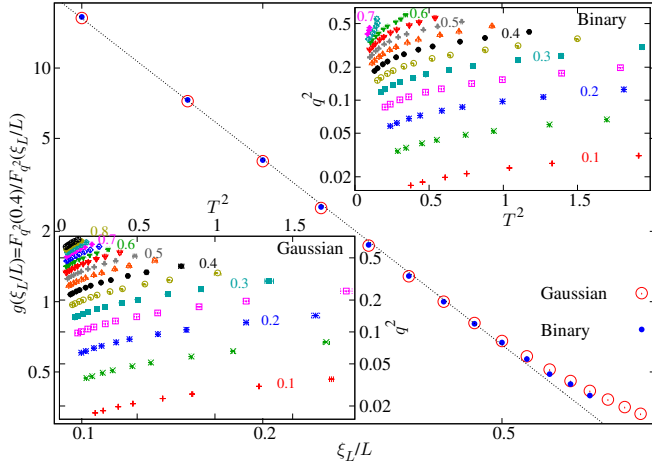


Figure 3. (color online) Order parameter  $\overline{q^2}$  computed at fixed values of  $\xi_L/L$  vs.  $[T_{\xi_L/L}^{(L)}]^2$ , for the binary (**upper inset**) and the Gaussian (**lower inset**) models. **Main:** universal scaling function  $g(\xi_L/L) = F_{q^2}(0.4)/F_{q^2}(\xi_L/L)$ , Eq. (4), as computed for the Gaussian (empty symbols) and the binary (full symbols) models. The function  $g(x = \xi_L/L)$  scales as  $1/x^2$  for small  $x$  (dashed line).

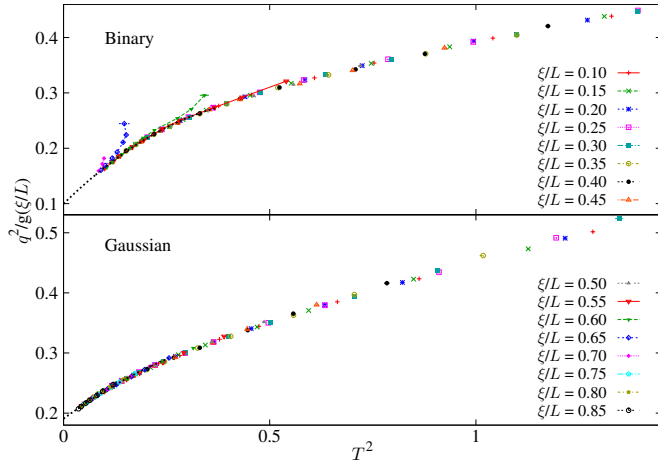


Figure 4. (color online) Scaling field  $[\hat{u}_h(T)]^2$  (from Eq. (4)) vs.  $[T_{\xi_L/L}^{(L)}]^2$ , as computed for the Gaussian (**top**) and the binary (**bottom**) models. The data collapses were obtained by multiplying the data in the two insets in Fig. 3 by the universal function  $g(\xi_L/L)$ , depicted in the main panel of Fig. 3. The dots are for the extrapolation to  $T^2 = 0$ . The binary model data show the crossover between the  $T = 0$  (small  $L$ ) and  $T > 0$  (large  $L$ ) regimes (see Fig. 1 and Refs. [33, 34]).

$L^{-1/\nu} F_{\xi}^{-1}(\xi_L/L)$ . Inverting this relation, one obtains  $T_{\xi_L/L}^{(L)} = d_1^{(\xi_L/L)} L^{-1/\nu} + d_3^{(\xi_L/L)} L^{-3/\nu} + d_5^{(\xi_L/L)} L^{-5/\nu} + \dots$ . Since  $1/\nu \approx 0.28$ , we expect annoying corrections to scaling due to the non-linearity of the scaling fields. Were  $\hat{u}_T(T)$  analytically known, we could easily get rid of these corrections. We shall not achieve this, but we shall get close to it.

In order to eliminate the unknown scaling function  $F_{\xi}$ ,

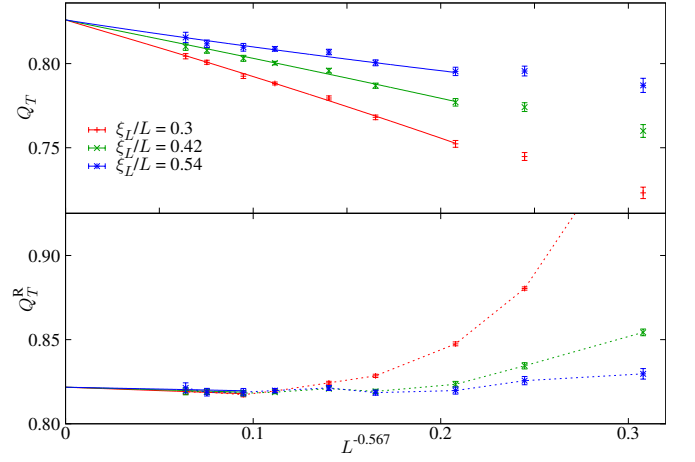


Figure 5. (color online) Computing  $\nu$  for the Gaussian model. Bare **top**, see Eq. (7)] and Renormalized **bottom**, Eq. (8) with  $\hat{u}_3 = -0.32$ ] temperature quotients at fixed  $\xi_L/L (= 0.3, 0.42, 0.54)$  as a function of  $L^{-2/\nu}$ . Continuous lines are our fits (see text), dotted lines are guides to eyes.

we compare couples of lattices of size  $L$  and  $2L$ :

$$Q_T(L) = \frac{T_{\xi_L/L}^{(2L)}}{T_{\xi_L/L}^{(L)}} = 2^{-1/\nu} \frac{1 + u_3 [T_{\xi_L/L}^{(L)}]^2 + \dots}{1 + u_3 [T_{\xi_L/L}^{(2L)}]^2 + \dots}. \quad (7)$$

In fact, see Fig. 5–top, scaling corrections are strong, and strongly dependent on  $\xi_L/L$ .

We can alleviate the situation by introducing a renormalized quotient

$$Q_T^R(L) = \frac{T_{\xi_L/L}^{(2L)}}{T_{\xi_L/L}^{(L)}} \frac{1 + \hat{u}_3 [T_{\xi_L/L}^{(2L)}]^2}{1 + \hat{u}_3 [T_{\xi_L/L}^{(L)}]^2}. \quad (8)$$

Setting  $\hat{u}_3 = u_3$  we would have  $Q_T^R(L) = 2^{1/\nu} + \mathcal{O}(u_5 L^{-4/\nu})$ . We have found that  $\hat{u}_3 = -0.32$  produces a negligible slope: the remaining corrections in Fig. 5–bottom are certainly of a different origin (either  $u_5$  terms, analytic corrections to scaling, or even  $L^{-\omega}$  terms).

We obtained a fit  $Q_T^R(L) = 2^{1/\nu} + d^{(\xi_L/L)} L^{-2/\nu}$  (i.e. we did *not* assume  $\hat{u}_3 = u_3$ ) finding

$$1/\nu = 0.283(6), \quad \chi^2/\text{dof} = 4.1/6 \quad (L_{\min} = 64). \quad (9)$$

Variations of 10% in  $\hat{u}_3$  change the  $1/\nu$  estimate by one third of the error bar. Furthermore, we can fit directly  $Q_T(L)$ , see Fig. 5–top. In this case, we need to introduce corrections quadratic in  $L^{-2/\nu}$ . We find a fair fit for  $L_{\min} = 16$  with  $1/\nu = 0.275(9)$ .

## VIII. CONCLUSIONS.

We have presented a high accuracy numerical simulation of the Edwards-Anderson spin glass model in 2D. We consider systems with binary and Gaussian random

couplings. By focusing on renormalized quantities we are able to bypass the peculiar temperature evolution dictated by the binary distribution. The Binder ratios at fixed  $\xi_L/L$  are fully compatible, in the precision given by our small statistical errors, with a single universality class. This analysis yields the first computation of the leading corrections to scaling exponent  $\omega$ . We identify the non-linearity of scaling fields as the major obstacle that impeded so far an accurate computation of critical quantities. We are able to give strong numerical evidence that the anomalous dimension  $\eta$  vanishes. We consider the temperature evolution for the Gaussian distribution, which is free of cross-over effects. We obtain a reliable direct estimate of  $\nu$ . Therefore, we are able to provide a stringent test of the generally assumed equivalence  $\theta = -1/\nu$ .

## IX. ACKNOWLEDGMENTS

This work was partially supported by the Ministerio de Ciencia y Tecnología (Spain) through Grant Nos. FIS2012-35719-C02, FIS2013-42840-P, by the Junta de Extremadura (Spain) through Grant No. GRU10158 (partially founded by FEDER).

### Appendix A: Parameters of simulations and fits

#### 1. Numerical simulations

The parameters describing our multi-spin coding simulations are given in Tables I and II. We treat temperature as a continuous variable, even if our data are obtained only in the temperature grid where our Parallel Tempering simulations take place. We solved this problem by using a standard cubic-spline interpolation. Note that data for neighboring temperatures are statistically correlated (because we use Parallel Tempering) which makes interpolation particularly easy in our case.

#### 2. Temperature fits

The computation of the scaling field  $\hat{u}_h(T)$  and of the scaling function  $F_{q^2}$ , depicted in Figs. 3 and 4, is based on a temperature fit. For each prescribed value of  $\xi_L/L$  and each system size  $L$ , we considered  $\overline{\langle q^2 \rangle}_{\xi_L/L}$  (namely the squared spin overlap as computed at  $T = T_{\xi_L/L}^{(L)}$ , the temperature needed to have  $\xi_L/L$  equal to its prescribed value in a system of size  $L$ ). For each fixed value of  $\xi_L/L$  we fitted  $\overline{\langle q^2 \rangle}_{\xi_L/L}$ , as computed for all our system sizes, to a second order polynomial in  $[T_{\xi_L/L}^{(L)}]^2$ . The fits were performed in the range  $0 < T^2 < T_{\max, \xi_L/L}^2$ . The values of  $T_{\max, \xi_L/L}^2$  were obtained with a simple algorithm: 1) For  $\xi_L/L = 0.1$  we took  $T_{\max, \xi_L/L}^2 = 0.8$ . 2) We increased

$L$	$N_{\text{samples}}$	$N_{\text{MCS}}$	$N_{\text{T}}$	$T_{\min}$	$T_{\max}$
4	25 600	320 000	14	0.20	1.5
4*	204 800	80 000	20	0.72	1.5
6	25 600	320 000	14	0.20	1.5
6*	204 800	80 000	20	0.65	1.5
8	25 600	320 000	14	0.20	1.5
8*	204 800	80 000	22	0.60	1.5
12	25 600	320 000	14	0.20	1.5
12*	204 800	80 000	19	0.53	1.5
16	25 600	320 000	14	0.20	1.5
16*	204 800	80 000	18	0.47	1.5
24	25 600	320 000	14	0.20	1.5
24*	204 800	80 000	16	0.45	1.5
32	25 600	128 000	14	0.20	1.5
32*	204 800	80 000	18	0.40	1.5
48	25 600	1 920 000	27	0.20	1.5
48*	204 800	160 000	27	0.35	1.5
64	25 600	640 000	26	0.25	1.5
64*	204 800	240 000	26	0.35	1.5
96	102 400	320 000	49	0.30	1.5
128	25 600	640 000	49	0.30	1.5

Table I. Details of the numerical simulations for the binary model. We show the simulation parameters for each lattice size  $L$ .  $N_{\text{samples}}$  is the number of simulated samples (in bunches of 128 samples, due to multi-spin coding).  $N_{\text{T}}$  is the number of temperatures that were used in parallel tempering, with maximum and minimum temperatures  $T_{\max}$  and  $T_{\min}$ , respectively. In general, temperatures were evenly spaced. However some system sizes appear twice in the table. In fact, we performed some higher accuracy simulations, marked by a \*, aiming to increase the accuracy in the computation of  $T_{\xi_L/L}^{(L)}$ , the temperature where  $\xi_L/L$  reaches a given prescribed value (see Fig. 1) and to improve the computation of  $\omega$  (see Fig. 2). For those extended runs, we increased the number of temperatures in the region where  $\xi_L/L > 0.3$ , in order to reduce the error for temperature interpolations. Finally,  $N_{\text{MCS}}$  is the number of Monte Carlo steps (MCS) used in each numerical simulation. Each MCS consisted of 10 Metropolis sweeps at fixed temperature, followed by a cluster update [60] and by a Parallel Tempering step [61, 62].

$\xi_L/L$  in steps of 0.05. 3) At each such step,  $T_{\max, \xi_L/L}^2$  was divided by 1.1.

The above procedure has general validity. However for the binary case at large  $\xi_L/L \geq 0.6$  our data are strongly affected by the crossover from the  $T > 0$  to the  $T = 0$  behavior [33, 34], illustrated in Figs. 1 and 3. In order to avoid as much as possible the effects of this crossover in the temperature window used in the fit, we employed  $T_{\max, \xi_L/L}^2 = 0.19, 0.13$  and  $0.11$  for  $\xi_L/L = 0.6, 0.65$  and  $0.7$ , respectively. Also for these three cases, the comparison with  $\xi_L/L = 0.4$  (needed to compute the scaling function  $g$  in Fig. 3) was done at  $0.8T_{\max, \xi_L/L}^2$ .

$L$	$N_{\text{samples}}$	$N_{\text{MCS}}$	$N_{\text{T}}$	$T_{\text{min}}$	$T_{\text{max}}$
4	204 800	160 000	31	0.1	1.5
6	204 800	160 000	31	0.1	1.5
8	204 800	160 000	31	0.1	1.5
12	204 800	160 000	31	0.1	1.5
16	204 800	160 000	31	0.1	1.5
24	204 800	160 000	31	0.1	1.5
32	204 800	320 000	31	0.1	1.5
48	204 800	160 000	27	0.2	1.5
64	25 600	320 000	53	0.2	1.5
96	25 600	480 000	41	0.2	0.7
128	25 600	800 000	41	0.2	0.7

Table II. Simulation details for the Gaussian model, as in Table I. Here the number of samples  $N_{\text{samples}}$  is given by the number of random choices of the absolute values of the couplings times 128 independent random choices of the coupling signs for each set of absolute values (see Sect. B).

## Appendix B: Multi spin coding the Gaussian model

This section is divided in two parts. We first explain how we define the multi spin coding algorithm with Gaussian couplings in B 1. Next, we assess in B 2 the statistical effectiveness of our algorithm.

### 1. The algorithm

It has been known for a long time how to perform the Metropolis update of a single spin using only Boolean operations (AND, XOR, etc.), provided that couplings are binary  $J_{\mathbf{x}\mathbf{y}} = \pm 1$ , see e.g. [56]. Besides, modern CPU perform synchronously independent Boolean operations for all the bits in a computer word.

Multi-spin coding is the fruitful combination of the above two observations: one codes, and simulates in parallel, as many different samples as the number of bits a word contains. Modern CPUs enjoy streaming extensions that allow to code in a word 128 (or even more) spins pertaining to the same site but to different samples. The most efficient version of our programs turns out to be the one with 128-bits words.

The situation changes, of course, when the couplings  $J_{\mathbf{x}\mathbf{y}}$  are drawn from a continuous distribution, such as a Gaussian. In fact, we are not aware of working multi-spin coding strategies when the coupling distribution is continuous. We explain now how we circumvented this problem [63].

Before describing our algorithm let us spell the standard Metropolis algorithm, phrased in a somewhat unusual (but fully orthodox) way. Imagine we are working at inverse temperature  $\beta = 1/T$ . When updating site  $\mathbf{x}$  we attempt to flip the spin  $\sigma_{\mathbf{x}} \rightarrow -\sigma_{\mathbf{x}}$ . Specifically,

1. We extract a random number  $R$  uniformly distributed in  $[0, 1)$ .
2. We compute the energy change  $\Delta E$  that the system would suffer if the spin  $\sigma_{\mathbf{x}}$  was flipped. In our case,  $\Delta E = 2 \sum_{\mathbf{y} \text{ neighbor of } \mathbf{x}} J_{\mathbf{x}\mathbf{y}} \sigma_{\mathbf{x}} \sigma_{\mathbf{y}}$
3. We reject the spin flip only if  $\exp(-\beta \Delta E) < R$ . Otherwise, we flip the spin.

So, we shall first get the random number  $R$ , then check if the actual  $\Delta E$  forces us to reject the spin-flip. Let us see how it works.

Let us call  $N_{\mathbf{x}}$  the set of the four nearest neighbors of  $\mathbf{x}$  in the square lattice endowed with periodic boundary conditions. For later use, let us also split the couplings into their absolute values and their signs  $J_{\mathbf{x}\mathbf{y}} = |J_{\mathbf{x}\mathbf{y}}| \text{sgn}(J_{\mathbf{x}\mathbf{y}})$ . The crucial observation is that for fixed  $|J_{\mathbf{x}\mathbf{y}}|$  the sum

$$S_{\mathbf{x}} = \sum_{\mathbf{y} \in N_{\mathbf{x}}} |J_{\mathbf{x}\mathbf{y}}| \text{sgn}(J_{\mathbf{x}\mathbf{y}}) \sigma_{\mathbf{x}} \sigma_{\mathbf{y}}, \quad (\text{B1})$$

can only take  $2^4 = 16$  different values, because each term of the sum in Eq. (B1) is a binary variable  $[\text{sgn}(J_{\mathbf{x}\mathbf{y}}) \sigma_{\mathbf{x}} \sigma_{\mathbf{y}} = \pm 1]$  and there are 4 neighboring sites  $\mathbf{y}$ . Of course,  $S_{\mathbf{x}} = \Delta E/2$  (recall the above description of the Metropolis algorithm). Now, let us name the 16 possible values of  $S_{\mathbf{x}}$  as

$$s_0 < s_1 < \dots < s_7 < 0 < s_8 < s_9 < \dots < s_{15}. \quad (\text{B2})$$

In fact, the symmetry of the problem ensures that  $s_7 = -s_8$ ,  $s_6 = -s_9$ , etc. Note also that having  $s_i = 0$  for some  $i$ , or  $s_i = s_k$  for a pair  $i$  and  $k$ , are zero-measure events.

Let us chose an (arbitrary) ordering for the four neighbors: South, East, North and West. We have  $S_{\mathbf{x}} = s_{15}$  when the four signs are  $\{\text{sgn}(J_{\mathbf{x}\mathbf{y}}) \sigma_{\mathbf{x}} \sigma_{\mathbf{y}}\}_{15} = \{+1, +1, +1, +1\}$ . Next, let us consider  $s_{14}$ . If the weakest link (i.e. smallest  $|J_{\mathbf{x}\mathbf{y}}|$ ) corresponded to (say) the East neighbor, then the array yielding  $s_{14}$  would be  $\{\text{sgn}(J_{\mathbf{x}\mathbf{y}}) \sigma_{\mathbf{x}} \sigma_{\mathbf{y}}\}_{14} = \{+1, -1, +1, +1\}$ . The groups of four signs are ordered in such away to produce decreasing values of the 16  $s_i$ 's. The eight groups  $\{\text{sgn}(J_{\mathbf{x}\mathbf{y}}) \sigma_{\mathbf{x}} \sigma_{\mathbf{y}}\}_{15}, \dots, \{\text{sgn}(J_{\mathbf{x}\mathbf{y}}) \sigma_{\mathbf{x}} \sigma_{\mathbf{y}}\}_8$  deserve special attention: if the current configuration takes one of these values, then the energy will *increase* upon flipping  $\sigma_{\mathbf{x}}$ . If the energy increases we shall be forced to reject the spin-flip (unless the random number turns out to be small enough).

With these definitions, the algorithm is easy to explain. We draw a random number  $0 \leq R < 1$  with uniform probability. The Metropolis update of site  $\mathbf{x}$  at inverse temperature  $\beta = 1/T$  can be cast as follows:

1. If  $R < e^{-2\beta s_{15}}$  we flip the spin  $\sigma_{\mathbf{x}} \rightarrow -\sigma_{\mathbf{x}}$ .
2. If  $e^{-2\beta s_{15}} < R < e^{-2\beta s_{14}}$  and the current configuration of the four signs turns out to be identical to the *forbidden* array  $\{\text{sgn}(J_{\mathbf{x}\mathbf{y}}) \sigma_{\mathbf{x}} \sigma_{\mathbf{y}}\}_{15}$  we let  $\sigma_{\mathbf{x}}$  unchanged. Otherwise, we reverse the spin.

3. If  $e^{-2\beta s_{14}} < R < e^{-2\beta s_{13}}$  we reverse  $\sigma_x$  unless the current configuration of the four signs is identical to one of the two configuration in the forbidden set:  $\{\text{sgn}(J_{xy})\sigma_x\sigma_y\}_{15}$  or  $\{\text{sgn}(J_{xy})\sigma_x\sigma_y\}_{14}$ .
4. If  $e^{-2\beta s_{13}} < R < e^{-2\beta s_{12}}$ , the forbidden set contains  $\{\text{sgn}(J_{xy})\sigma_x\sigma_y\}_{15}$ ,  $\{\text{sgn}(J_{xy})\sigma_x\sigma_y\}_{14}$  and  $\{\text{sgn}(J_{xy})\sigma_x\sigma_y\}_{13}$ . We reverse  $\sigma_x$  unless the current signs configuration is contained in the forbidden set.
5. The same scheme apply to the other intervals, up to  $e^{-2\beta s_8} < R$ . In this extremal case, the forbidden set contains all the energy-increasing configurations of the four signs:  $\{\text{sgn}(J_{xy})\sigma_x\sigma_y\}_{15}, \dots, \{\text{sgn}(J_{xy})\sigma_x\sigma_y\}_8$ .

We can bypass the use of floating point arithmetics by using a look up table. For each of the  $L^2$  sites of the system we need to keep in our table the eight probability thresholds

$$e^{-2\beta s_{15}} < e^{-2\beta s_{14}} < \dots < e^{-2\beta s_8},$$

and the corresponding eight *sometimes forbidden* four-signs configurations

$$\{\text{sgn}(J_{xy})\sigma_x\sigma_y\}_{15}, \{\text{sgn}(J_{xy})\sigma_x\sigma_y\}_{14}, \dots, \{\text{sgn}(J_{xy})\sigma_x\sigma_y\}_8.$$

The look-up table is entirely determined by the absolute values of the couplings  $|J_{xy}|$ .

At this point, our multi-spin coding solution is straightforward. We chose to code 128 different samples in each computer word. We set randomly and independently the *sign* of each of the  $128 \times 2 \times L^2$  couplings,  $\text{sgn}(J_{xy}) = \pm 1$  with 50% probability. However, we only extract  $2 \times L^2$  independent absolute values  $|J_{xy}|$  from the Gaussian distribution. This  $|J_{xy}|$  is common to all the 128 bits in the computer word that codes the bond between lattice sites  $x$  and  $y$ .

## 2. The effective number of samples

As far as we know, our multi-spin coding scheme is new and it has never been tested. Therefore, it is useful to investigate its effectiveness.

Let us consider a Monte Carlo simulation long enough to make thermal errors negligible as compared to sample to sample fluctuations [64]. Let us now simulate  $N_S$  *independent* samples, in order to compute the expectation value  $\langle O \rangle$  for an observable  $O$ . For instance,  $O$  could be the energy density  $e = H/L^2$ , or the squared spin overlap  $q^2$ .

Our estimate will suffer from a statistical error  $\Delta_O$  of typical (squared) size

$$\Delta_O^2 = \frac{\text{Var}(O)}{N_S}, \quad (\text{B3})$$

where  $\text{Var}(O) = \overline{\langle O \rangle^2} - \overline{\langle O \rangle}^2$  is the variance of  $O$ .

We want to analyze a situation in which the coupling absolute values  $|J_{xy}|$  are fixed while we average over many different coupling signs. It will be useful to recall some simple notions about conditional probabilities (the same ideas were heavily used in Refs. [65, 66]). Let  $\langle O \rangle_{|J|, \text{sgn}(J)}$  be the thermal expectation of  $O$  for a given sample. We split the couplings in their absolute values and their signs  $J_{xy} = |J_{xy}| \text{sgn}(J_{xy})$ . The conditional expectation value of  $\langle O \rangle_{|J|, \text{sgn}(J)}$ , given the absolute values for the couplings, is

$$E(\langle O \rangle | |J|) = \frac{1}{2^{N_B}} \sum_{\{\text{sgn}(J)\}} \langle O \rangle_{|J|, \text{sgn}(J)}, \quad (\text{B4})$$

where  $N_B = 2L^2$  is the number of bonds in the square lattice and the sum extends to the  $2^{N_B}$  equally probable sign-assignments for the couplings. The relationship with the standard expectation values is straightforward

$$E(O) \equiv \overline{\langle O \rangle} = \int D|J| E(\langle O \rangle | |J|), \quad (\text{B5})$$

where  $\int D|J|$  indicates the average taken with respect to the absolute value of the couplings.

The variance can be treated in a similar way. The variance induced by the absolute values is

$$\text{Var}_{|J|}(O) = \int D|J| \left( E(\langle O \rangle | |J|) - E(O) \right)^2. \quad (\text{B6})$$

Instead, the  $|J|$ -averaged variance induced by the signs is

$$\begin{aligned} \text{Var}_{\text{sgn}(J)}(O) &= \\ \int D|J| \frac{1}{2^{N_B}} \sum_{\{\text{sgn}(J)\}} \left( \langle O \rangle_{|J|, \text{sgn}(J)} - E(\langle O \rangle | |J|) \right)^2. \end{aligned} \quad (\text{B7})$$

It is straightforward to show that

$$\text{Var}(O) = \text{Var}_{|J|}(O) + \text{Var}_{\text{sgn}(J)}(O). \quad (\text{B8})$$

We are finally ready to discuss our multi-spin coding simulation. Imagine we simulate  $N_{|J|}$  choices of the absolute values for the couplings. Our squared statistical error is

$$\Delta_{O, \text{MSC}}^2 = \frac{1}{N_{|J|}} \left[ \text{Var}_{|J|}(O) + \frac{\text{Var}_{\text{sgn}(J)}(O)}{128} \right]. \quad (\text{B9})$$

However, the comparison with Eq. (B3) suggests us to define the effective number of samples in our 128 bits,  $N_{\text{eff}, O}$ , through

$$\Delta_{O, \text{MSC}}^2 = \frac{\text{Var}(O)}{N_{|J|} N_{\text{eff}, O}} \quad (\text{B10})$$

The combination of Eqs. (B8) and (B10) tells us that

$$N_{\text{eff}, O} = 128 \frac{1+z}{128+z} \quad \text{where} \quad z = \frac{\text{Var}_{\text{sgn}(J)}(O)}{\text{Var}_{|J|}(O)}. \quad (\text{B11})$$



$L$	$\xi_L$	$T$	$N_S$	$N_{ J }$	$N_{\text{eff},e}$	$N_{\text{eff},q^2}$	$N_{\text{eff},\xi_L}$	$N_{\text{eff},U_4}$
8	3.031(9)	0.7	200	200	1.1	8.8	11.3	11.2
64	4.599(12)	0.7	200	200	1.4	8.0	7.0	8.1
8	8.581(19)	0.2	200	200	0.9	34.2	42.4	58.6
48	35.86(4)	0.2	200	1600	1.4	89.2	106.4	110.6

Table III. Numerical estimation of the effective number of independent samples in a 128 bits computer word, from Eq. (B13). We give results obtained under different dynamical conditions for the following observables: internal energy  $N_{\text{eff},e}$ , squared overlap  $N_{\text{eff},q^2}$ , correlation length  $N_{\text{eff},\xi_L}$ , and Binder ratio  $N_{\text{eff},U_4}$ . We somehow abuse notation when applying Eq. (B13) to quantities such as the correlation length  $\xi_L$  or the Binder ratio  $U_4$ , which are computed as non-linear functions of mean values of direct observables. The statistical error in the computation of  $N_{\text{eff}}$  is below 10%.

Therefore, the effective number of samples in our 128 bits computer word is bounded as

$$1 < N_{\text{eff},O} < 128. \quad (\text{B12})$$

If the variance ratio  $z$  is small, then  $N_{\text{eff},O} \approx 1$  and we will gain nothing by multi-spin coding. On the other hand, if the statistical fluctuations induced by the signs dominate,  $z$  will be large and we shall approach to the optimal efficiency  $N_{\text{eff},O} = 128$ .

The problem to assess the effectiveness of our approach beforehand is that estimating the variances  $\text{Var}_{|J|}(O)$  or  $\text{Var}_{\text{sgn}(J)}(O)$  is not easy. However, we can do it by running two different kinds of numerical simulations. On the one hand we can perform simulations with  $N_S$  independent couplings. On the other hand, we use multi-spin coding in a simulation with  $N_{|J|}$  independent choices of the absolute values for the couplings. Numerical estimates of the statistical errors,  $\tilde{\Delta}_O$  and  $\tilde{\Delta}_{O,\text{MSC}}$ , can be obtained in a standard way. Then, Eqs. (B3) and (B10) tell us that

$$N_{\text{eff},O} \approx \frac{\tilde{\Delta}_O^2}{\tilde{\Delta}_{O,\text{MSC}}^2} \frac{N_S}{N_{|J|}}. \quad (\text{B13})$$

Some numerical experiments, described in Table III, convinced us that our multi-spin coding is extremely useful when computing long-distance observables, particularly when the correlation length is large  $\xi_L \gg 1$  and the system size increases. On the other hand, when computing short distance observables (such as the internal energy),  $N_{\text{eff},O}$  turns out to be disappointingly close to one. Fortunately, for long-distance quantities, such as the Binder parameter at  $\xi \approx 36$ , we have an effective number of samples as large as  $N_{\text{eff},U_4} \approx 111$ .

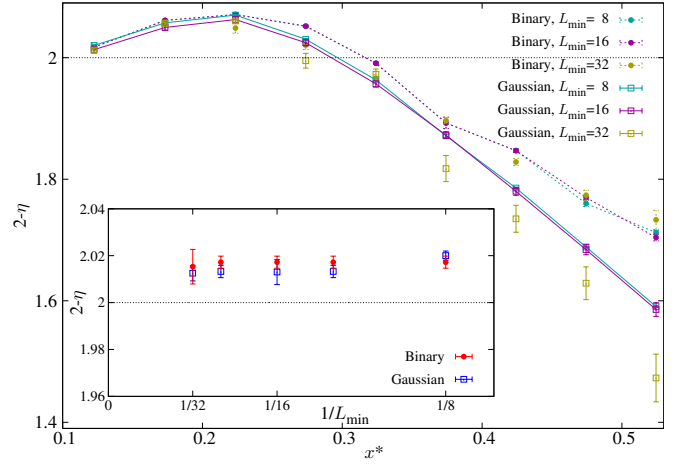


Figure 6. Effective value of  $2 - \eta$  as obtained from Eq. (C2) versus  $x^*$  (which is the geometric mean of the two values of  $\xi_L/L$  involved in the computation of  $\eta$ ). We show estimations for several values of the minimal size included in the analysis,  $L_{\min}$ . Data for the binary model obtained with the same value of  $L_{\min}$  are connected by dashed lines (continuous lines in the case of Gaussian distributed couplings). **Inset:** For the smallest argument  $x^*$  that we reach in our simulations, we investigate the dependency of  $2 - \eta$  on  $L_{\min}$ .

### Appendix C: Computing the anomalous dimension

We have seen that

$$\overline{g^2} = [\hat{u}_h(T)]^2 F_{q^2}(\xi_L/L), \quad g(\xi_L/L) = \frac{F_{q^2}(0.4)}{F_{q^2}(\xi_L/L)}.$$

Let us define  $x \equiv \xi_L/L$ . The universal scaling function  $g(x)$  was depicted in Fig. 3. We shall employ it here, to obtain a quantitative bound on the anomalous dimension  $\eta$ .

If we take the  $L \rightarrow \infty$  limit at fixed  $x$ , for small  $x$  we obtain the scaling law

$$g(x) \propto \frac{1}{x^{2-\eta}}. \quad (\text{C1})$$

Our procedure is as follows. We first determine  $g(x, L_{\min})$  by computing the scaling function  $g(x)$  as explained before, but restricting the analysis to data from system sizes  $L \geq L_{\min}$ . We then consider pairs of arguments  $x_1$  and  $x_2$  (consecutive points in the  $x$  grid where we compute  $g(x)$ , see Fig. 3) and obtain the effective estimators

$$2 - \eta(x^*) = \frac{\log[g(x_1, L_{\min})/g(x_2, L_{\min})]}{\log[x_2/x_1]}, \quad x^* \equiv \sqrt{x_1 x_2}, \quad (\text{C2})$$

that are shown in Fig. 6.

The estimations depicted in Fig. 6 depend on everything they could: on the disorder distribution, on  $L_{\min}$  and on  $x^*$ . However, for small  $x^*$  the dependency on  $L_{\min}$  and on the disorder distribution become negligible within our better than 1% accuracy (see Fig. 6—insert) [67].



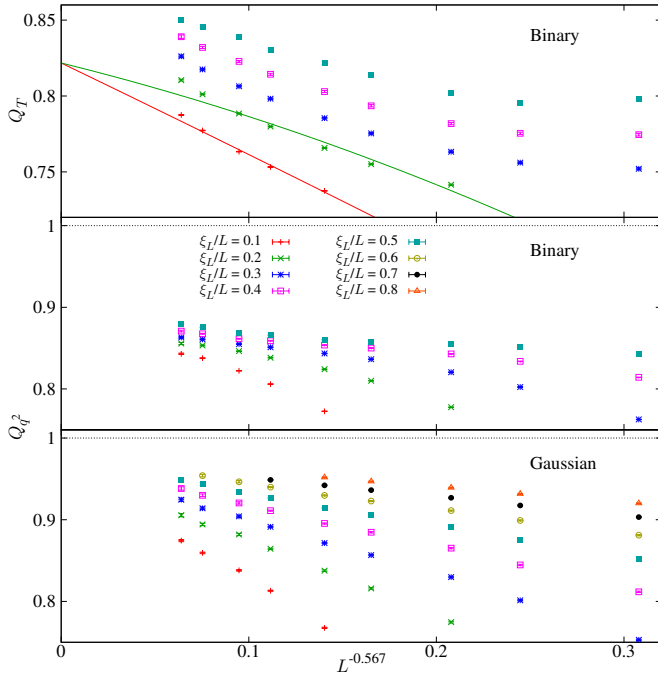


Figure 7. The effective, size dependent critical exponents  $\nu$  [**Top:** binary model.  $Q_T$  is defined in Eq. D1.] and the anomalous dimension  $\eta$  (**Middle:** binary model. **Bottom:** Gaussian model). The quotient  $Q_{q^2}$  is defined in Eq. (D2) and analyzed in Eq. (D3).

It is obvious from Fig. 6 that effects from different origin compete: statistical errors and systematic errors due to  $x^*$  been too large (or to  $L_{\min}$  being too small). However, we have an additional hint: we expect  $\eta = 0$  for the Gaussian model. But we see identical 1% deviations from  $2 - \eta = 2$  for Gaussian and for binary couplings. Thus we regard the small difference in the inset in Fig. 6 as an estimation of the combined errors (systematic and statistical) that we suffer. We can safely summarize our findings as

$$|\eta_{\text{binary}}| < 0.02. \quad (\text{C3})$$

#### Appendix D: Traditional analysis

For sake of completeness, we include here the results of a traditional analysis, based on scaling laws as a function of the system temperature. These results give a flavor of how severe are the problems caused by the non-linear scaling fields.

The difficulties encountered in the computation of the thermal exponent  $\nu$  are explained in Sect. VII. One can compute it from the comparison of temperatures  $T_{\xi_L/L}^{(L)}$  for lattices  $L$  and  $2L$ :

$$Q_T(L) = \frac{T_{\xi_L/L}^{(2L)}}{T_{\xi_L/L}^{(L)}} = 2^{-1/\nu}(1 + \dots). \quad (\text{D1})$$

When computing this ratio for the Binary model, see Fig. 7–top, the scaling corrections come from a number of different source. We have, of course, the corrections due to the scaling field  $\hat{u}_T$  that were discussed in Sect. VII. Yet, we also have strong corrections of order  $\mathcal{O}(L^{-\omega})$  [instead, for the Gaussian model we are fortunate to have tiny, probably negligible,  $\mathcal{O}(L^{-\omega})$  corrections, see Fig. 2]. We also have to deal with the crossover between  $T = 0$  and  $T > 0$  behaviors [33, 34] (for a fixed variation range of  $L$ , the crossover appears when increasing  $\xi_L/L$ ). In fact, we know that some of these scaling corrections are of similar magnitude: those arising from  $\hat{u}_T$  should be of order  $L^{-2/\nu}$  with  $1/\nu = 0.283(6)$  while  $\omega = 0.75(10)(5)$ . Disentangling the effects of the three sources of corrections to scaling will require a strong analytical guidance. Probably, simulating much larger systems, which is possible using special methods [68], will be useful.

As for the anomalous dimension, the traditional approach would start from the quotients of  $\langle q^2 \rangle$  at fixed  $\xi_L/L$ , as computed for  $L$  and  $2L$ :

$$Q_{q^2}(L) = \frac{\langle q^2 \rangle(2L, T_{\xi_L/L}^{(2L)})}{\langle q^2 \rangle(L, T_{\xi_L/L}^{(L)})}. \quad (\text{D2})$$

Barring scaling corrections, this quotient should behave as  $2^{-\eta}$ . Therefore, for very large  $L$ ,  $Q_{q^2}(L)$  should tend to one. The reason for this unfavorable behavior is that (ignoring all sort of scaling corrections) this ratio actually behaves as

$$Q_{q^2}(L) = 2^{-\eta} \left( \frac{\hat{u}_h(T_{\xi_L/L}^{(2L)})}{u_h(T_{\xi_L/L}^{(L)})} \right)^2. \quad (\text{D3})$$

In fact, in the thermodynamic limit the two temperatures  $T_{\xi_L/L}^{(2L)}$  and  $T_{\xi_L/L}^{(L)}$  tend to  $T = 0$ , making the ratio of scaling fields in Eq. (D3) irrelevant. However, our data are far away from this limit, as shown in Fig. 4.

In fact, we know that  $T_{\xi_L/L}^{(2L)} < T_{\xi_L/L}^{(L)}$  and that  $\hat{u}_h$  is an increasing function (recall again Fig. 4). It follows that the ratio of scaling functions in Eq. (D3) is smaller than one, which mimics a slightly positive *effective* anomalous dimension, see Fig 7–middle and bottom.

- [1] S. F. Edwards and P. W. Anderson, Journal of Physics F: Metal Physics **5**, 965 (1975).
- [2] K. Binder and A. P. Young, Rev. Mod. Phys. **58**, 801

(1986).

- [3] M. Mézard, G. Parisi, and M. Virasoro, *Spin-Glass Theory and Beyond* (World Scientific, Singapore, 1987).

- [4] K. Fisher and J. Hertz, *Spin Glasses* (Cambridge University Press, Cambridge England, 1991).
- [5] A. P. Young, *Spin Glasses and Random Fields* (World Scientific, Singapore, 1998).
- [6] M. Mézard and A. Montanari, *Information, Physics, and Computation* (OUP Oxford, Oxford, UK, 2009).
- [7] K. Binder and W. Kob, *Glassy Materials and Disordered Solids. An Introduction to Their Statistical Mechanics* (World Scientific, Singapore, 2011).
- [8] S. Kirkpatrick, Phys. Rev. B **16**, 4630 (1977).
- [9] I. Morgenstern and K. Binder, Phys. Rev. B **22**, 288 (1980).
- [10] J. A. Blackman, Phys. Rev. B **26**, 4987 (1982).
- [11] W. L. McMillan, Phys. Rev. B **28**, 5216 (1983).
- [12] H. F. Cheung and W. L. McMillan, Journal of Physics C: Solid State Physics **16**, 7027 (1983).
- [13] R. N. Bhatt and A. P. Young, in *Heidelberg Colloquium on Glassy Dynamics*, Lecture Notes in Physics No. 275, edited by J. L. van Hemmen and I. Morgenstern (Springer, Berlin, 1987).
- [14] R. R. P. Singh and S. Chakravarty, Phys. Rev. Lett. **57**, 245 (1986).
- [15] J.-S. Wang and R. H. Swendsen, Phys. Rev. B **38**, 4840 (1988).
- [16] H. Freund and P. Grassberger, Journal of Physics A: Mathematical and General **21**, L801 (1988).
- [17] H. Freund and P. Grassberger, Journal of Physics A: Mathematical and General **22**, 4045 (1989).
- [18] J. A. Blackman and J. Poulter, Phys. Rev. B **44**, 4374 (1991).
- [19] B. A. Berg and T. Celik, Phys. Rev. Lett. **69**, 2292 (1992).
- [20] L. Saul and M. Kardar, Phys. Rev. E **48**, R3221 (1993).
- [21] L. Saul and M. Kardar, Nuclear Physics B **432**, 641 (1994).
- [22] H. Rieger, L. Santen, U. Blasum, M. Diehl, M. Jünger, and G. Rinaldi, Journal of Physics A: Mathematical and General **29**, 3939 (1996).
- [23] H. Rieger, L. Santen, U. Blasum, M. Diehl, and M. Jünger, Journal of Physics A: Mathematical and General **30**, 8795 (1997).
- [24] A. K. Hartmann and A. P. Young, Phys. Rev. B **64**, 180404 (2001).
- [25] A. C. Carter, A. J. Bray, and M. A. Moore, Phys. Rev. Lett. **88**, 077201 (2002).
- [26] C. Amoruso, E. Marinari, O. C. Martin, and A. Pagnani, Phys. Rev. Lett. **91**, 087201 (2003).
- [27] J. Lukic, A. Galluccio, E. Marinari, O. C. Martin, and G. Rinaldi, Phys. Rev. Lett. **92**, 117202 (2004).
- [28] T. Jörg, J. Lukic, E. Marinari, and O. C. Martin, Phys. Rev. Lett. **96**, 237205 (2006).
- [29] J. Lukic, E. Marinari, O. C. Martin, and S. Sabatini, Journal of Statistical Mechanics: Theory and Experiment **2006**, L10001 (2006).
- [30] F. Liers, J. Lukic, E. Marinari, A. Pelissetto, and E. Vicari, Phys. Rev. B **76**, 174423 (2007).
- [31] H. G. Katzgraber, L. W. Lee, and I. A. Campbell, Phys. Rev. B **75**, 014412 (2007).
- [32] F. Parisen Toldin, A. Pelissetto, and E. Vicari, Phys. Rev. E **82**, 021106 (2010).
- [33] C. K. Thomas, D. A. Huse, and A. A. Middleton, Phys. Rev. Lett. **107**, 047203 (2011), arXiv:1103.1946.
- [34] F. Parisen Toldin, A. Pelissetto, and E. Vicari, Phys. Rev. E **84**, 051116 (2011).
- [35] T. Jörg and F. Krzakala, J. Stat. Mech. Theor. Exp. , L01001 (2012).
- [36] P. H. Lundow and I. A. Campbell, “The bimodal and gaussian ising spin glasses in dimension two revisited,” (2015), arXiv:1506.07141.
- [37] S. Guchhait and R. Orbach, Phys. Rev. Lett. **112**, 126401 (2014).
- [38] S. Guchhait, G. G. Kenning, R. L. Orbach, and G. F. Rodriguez, Phys. Rev. B **91**, 014434 (2015).
- [39] S. Guchhait and R. L. Orbach, Phys. Rev. B **92**, 214418 (2015).
- [40] N. G. Fytas and V. Martín-Mayor, Phys. Rev. Lett. **110**, 227201 (2013).
- [41] F. Belletti, M. Cotallo, A. Cruz, L. A. Fernandez, A. Gordillo-Guerrero, M. Guidetti, A. Maiorano, F. Mantovani, E. Marinari, V. Martín-Mayor, A. M. Sudupe, D. Navarro, G. Parisi, S. Perez-Gaviro, J. J. Ruiz-Lorenzo, S. F. Schifano, D. Sciretti, A. Tarancon, R. Tripiccone, J. L. Velasco, and D. Yllanes (Janus Collaboration), Phys. Rev. Lett. **101**, 157201 (2008), arXiv:0804.1471.
- [42] F. Belletti, A. Cruz, L. A. Fernandez, A. Gordillo-Guerrero, M. Guidetti, A. Maiorano, F. Mantovani, E. Marinari, V. Martín-Mayor, J. Monforte, A. Muñoz Sudupe, D. Navarro, G. Parisi, S. Perez-Gaviro, J. J. Ruiz-Lorenzo, S. F. Schifano, D. Sciretti, A. Tarancon, R. Tripiccone, and D. Yllanes (Janus Collaboration), J. Stat. Phys. **135**, 1121 (2009), arXiv:0811.2864.
- [43] L. A. Fernández and V. Martín-Mayor, Phys. Rev. B **91**, 174202 (2015).
- [44] M. Hasenbusch, A. Pelissetto, and E. Vicari, J. Stat. Mech. **2008**, L02001 (2008).
- [45] When the critical temperature,  $T_c$ , is nonzero the problems caused by the non-linear scaling fields can be bypassed using a standard analysis [49, 69, 70]. In fact in 3D spin glasses [71] one compares data from different system sizes at the *same* temperature, namely  $T_c$ , which cures most of the problems.
- [46] F. Cooper, B. Freedman, and D. Preston, Nucl. Phys. B **210**, 210 (1982).
- [47] M. Palassini and S. Caracciolo, Phys. Rev. Lett. **82**, 5128 (1999), arXiv:cond-mat/9904246.
- [48] H. G. Ballesteros, A. Cruz, L. A. Fernandez, V. Martín-Mayor, J. Pech, J. J. Ruiz-Lorenzo, A. Tarancon, P. Tellez, C. L. Ullod, and C. Ungil, Phys. Rev. B **62**, 14237 (2000), arXiv:cond-mat/0006211.
- [49] D. J. Amit and V. Martín-Mayor, *Field Theory, the Renormalization Group and Critical Phenomena*, 3rd ed. (World Scientific, Singapore, 2005).
- [50] J. Salas and A. D. Sokal, Journal of Statistical Physics **98**, 551 (2000).
- [51] The relationship between  $h$  and the “magnetic field”  $h_q$  coupled to the spin overlap is  $h_q = h^2 + \mathcal{O}(h^4)$ .
- [52] The universality of the scaling functions in  $D = 3$  spatial dimensions was carefully analyzed in [72].
- [53] G. Parisi, Journal of Statistical Physics **23**, 49 (1980).
- [54] S. Caracciolo, R. G. Edwards, S. J. Ferreira, A. Pelissetto, and A. D. Sokal, Phys. Rev. Lett. **74**, 2969 (1995).
- [55] S. Caracciolo, R. G. Edwards, A. Pelissetto, and A. D. Sokal, Phys. Rev. Lett. **75**, 1891 (1995).
- [56] M. E. J. Newman and G. T. Barkema, *Monte Carlo Methods in Statistical Physics* (Clarendon Press, Oxford, 1999).

- [57] The elementary Monte Carlo step consisted of 10 Metropolis sweeps at fixed temperature, followed by a cluster update [60] and by a parallel tempering step [61, 62]. We consider two sets of two real replicas for each temperatures. The cluster updates are performed only within each set (overlaps are computed by taking a pair of statistically independent configurations, each from one set). We performed a stringent equilibration test, that takes into account the statistical correlation when comparing the last logarithmic bins [73].
- [58] Data for the Gaussian model can be fit as well with a sub-leading correction term  $L^{-2\omega}$ , rather than with the  $L^{-2}$  term we use in Eq. (5). With either sub-leading term we found that the leading corrections to the Gaussian data vanish within numerical accuracy.
- [59] The tentative estimate of ref. [22] was later found to be problematic [23].
- [60] J. Houdayer, The European Physical Journal B - Condensed Matter and Complex Systems **22**, 479 (2001).
- [61] K. Hukushima and K. Nemoto, J. Phys. Soc. Japan **65**, 1604 (1996), arXiv:cond-mat/9512035.
- [62] E. Marinari, in *Advances in Computer Simulation*, edited by J. Kerstész and I. Kondor (Springer-Verlag, 1998).
- [63] Another general solution is to use a discrete approximation to the Gaussian distribution, such as the Gaussian-Hermite quadrature [74]. For instance, in Refs. [75, 76] a Gaussian-distributed magnetic field was simulated in this way.
- [64] This situation is not desirable [77], but it is almost automatically enforced by the standard thermalization tests for spin-glasses [73].
- [65] R. Alvarez Baños, A. Cruz, L. A. Fernandez, J. M. Gil-Narvion, A. Gordillo-Guerrero, M. Guidetti, A. Maiorano, F. Mantovani, E. Marinari, V. Martín-Mayor, J. Monforte-Garcia, A. Muñoz Sudupe, D. Navarro, G. Parisi, S. Perez-Gaviro, J. J. Ruiz-Lorenzo, S. F. Schifano, B. Seoane, A. Tarancon, R. Tripiccione, and D. Yllanes (Janus Collaboration), J. Stat. Mech. **2010**, P06026 (2010), arXiv:1003.2569.
- [66] M. Baity-Jesi, R. A. Baños, A. Cruz, L. A. Fernandez, J. M. Gil-Narvion, A. Gordillo-Guerrero, D. Iniguez, A. Maiorano, M. F., E. Marinari, V. Martín-Mayor, J. Monforte-Garcia, A. Muñoz Sudupe, D. Navarro, G. Parisi, S. Perez-Gaviro, M. Pivanti, F. Ricci-Tersenghi, J. J. Ruiz-Lorenzo, S. F. Schifano, B. Seoane, A. Tarancon, R. Tripiccione, and D. Yllanes, J. Stat. Mech. **2014**, P05014 (2014), arXiv:1403.2622.
- [67] For  $L_{\min} = 32$ , the automated selection of  $T_{\max, \xi_L/L}^2$  for the fits discussed in section A 2 does not result into a good data collapse. For instance, for Gaussian couplings,  $\xi_L/L = 0.1$  and  $L_{\min} \geq 32$  one needs to chose  $T_{\max, \xi_L/L}^2 = 0.53$  (rather than 0.8, as we choose for smaller  $L_{\min}$ ).
- [68] C. K. Thomas and A. A. Middleton, Phys. Rev. E **87**, 043303 (2013), arXiv:1301.1252.
- [69] M. Nightingale, Physica A: Statistical Mechanics and its Applications **83**, 561 (1976).
- [70] H. G. Ballesteros, L. A. Fernandez, V. Martín-Mayor, and A. Muñoz Sudupe, Phys. Lett. B **378**, 207 (1996), arXiv:hep-lat/9511003.
- [71] M. Baity-Jesi, R. A. Baños, A. Cruz, L. A. Fernandez, J. M. Gil-Narvion, A. Gordillo-Guerrero, D. Iniguez, A. Maiorano, F. Mantovani, E. Marinari, V. Martín-Mayor, J. Monforte-Garcia, A. Muñoz Sudupe, D. Navarro, G. Parisi, S. Perez-Gaviro, M. Pivanti, F. Ricci-Tersenghi, J. J. Ruiz-Lorenzo, S. F. Schifano, B. Seoane, A. Tarancon, R. Tripiccione, and D. Yllanes (Janus Collaboration), Phys. Rev. B **88**, 224416 (2013), arXiv:1310.2910.
- [72] T. Jörg, Phys. Rev. B **73**, 224431 (2006).
- [73] L. A. Fernandez, A. Maiorano, E. Marinari, V. Martín-Mayor, D. Navarro, D. Sciretti, A. Tarancon, and J. L. Velasco, Phys. Rev. B **77**, 104432 (2008), arXiv:0710.4246.
- [74] M. Abramowitz and I. A. Stegun, *Handbook of Mathematical Functions: with Formulas, Graphs, and Mathematical Tables.*, ninth ed. (Dover Publications, New York, 1972).
- [75] L. Leuzzi, G. Parisi, F. Ricci-Tersenghi, and J. J. Ruiz-Lorenzo, Phys. Rev. Lett. **103**, 267201 (2009), arXiv:0811.3435.
- [76] M. Baity-Jesi, R. A. Baños, A. Cruz, L. A. Fernandez, J. M. Gil-Narvion, A. Gordillo-Guerrero, D. Iniguez, A. Maiorano, M. F., E. Marinari, V. Martín-Mayor, J. Monforte-Garcia, A. Muñoz Sudupe, D. Navarro, G. Parisi, S. Perez-Gaviro, M. Pivanti, F. Ricci-Tersenghi, J. J. Ruiz-Lorenzo, S. F. Schifano, B. Seoane, A. Tarancon, R. Tripiccione, and D. Yllanes, Phys. Rev. E **89**, 032140 (2014), arXiv:1307.4998.
- [77] H. G. Ballesteros, L. A. Fernandez, V. Martín-Mayor, A. Muñoz Sudupe, G. Parisi, and J. J. Ruiz-Lorenzo, Nucl. Phys. B **512**, 681 (1998).